Influence of multiple sills upon internal wave generation and the implications for mixing

Jiuxing Xing and Alan M Davies

Proudman Oceanographic Laboratory,

6 Brownlow Street,

Liverpool L3 5DA, UK.

Abstract

A cross sectional non-hydrostatic model of a fjord is used to examine to what extent the internal tide is modified by two closely spaced sills. The model is forced with an M_2 barotropic tide and internal tides, unsteady lee waves and a jet are generated at the sills. In contrast to an isolated sill, calculations with two closely spaced sills show that the presence of the second sill leads to standing internal wave generation with associated changes in wave spectrum and Richardson number in the inter sill region. Associated with these there is a cascade of energy towards short waves leading to enhanced mixing between the sills. This increase in mixing is consistent with enhanced mixing between closely spaced sills found in observations. It is also relevant to enhanced oceanic mixing, and suggest that future mixing measurements should focus on these regions.

1. Introduction

The problem of the energy cascade from meteorological or tidal forcing to small scale internal waves and eventually mixing in the ocean has received significant attention in recent years. This is because just how and where this mixing takes place has important implications for the meridional circulation of the ocean. In terms of meteorologically induced mixing, calculations have shown that wind forcing in regions of horizontally varying vorticity (e.g. Xing and Davies 2005, Zhai et al., 2005) produces an enhancement in local mixing, and change in the internal wave spectrum. Consequently the determination of the internal wave spectral response of a model and associated changes in Richardson number (R_i) is as important in modelling as in field measurements (e.g. Van Haren et al., 2002).

In the case of tidal forcing, when the topographic length scale is small compared to the tidal excursion, (e.g. sills at the entrance to fjords) the processes are highly non-linear (Vlasenko et al., 2005) and besides generating an internal tide at the same frequency as the barotropic tide, waves such as lee waves, solitons and solibores are produced with much higher frequencies. As shown by Xing and Davies (2006) (hereafter XD06) small scale topographic features can produce a cascade of energy to higher frequencies and mixing.

Although recently there has been a major focus on modelling and measuring (New and Da Silva 2002) internal tides in oceanic regions and at sills the emphasis on understanding internal tide generation has focused on isolated topography e.g. a single seamount or a single sill (XD06). However recent measurements between two closely spaced sills in a fjord have shown that there is increased mixing in such locations (Johnsson et al., 2007).

Here a process study using an idealised cross sectional model of a fjord, initially with one sill and subsequently with two sills having an inter-sill distance comparable to that of the Ringdals fjord – Idefjord system (Johnsson et al., 2007) namely 1.5km, is used to examine to what extent the internal tide in the inter-sill region between the two sills differs from that generated at a single sill. In particular changes in the internal wave spectrum due to internal wave reflection and

generation of higher harmonics are examined. Changes in the Richardson number distribution are also considered and implications for internal wave mixing between the sills are discussed. Calculations suggest that internal wave trapping between the sills is the reason for the enhanced mixing found in observations. This is discussed in a final section, as are the implications for mixing in oceanic situations with closely spaced topography. The importance of this oceanic mixing in these critical regions in terms of oceanic circulation and the need to make fine scale measurements (Van Haren et al., 2002) in such areas is also discussed.

2. Model and calculations.

2.1 Model

Following on from the use of the MITgcm model to study mixing at a single sill (see XD06, and references therein for model details) the same model is used here. In the present study two identical sills are used. In order to determine how the internal tide generated at two sills differs from that produced at a single sill, initially calculations are performed with a single sill at x = 0 (Fig 1a). Subsequently calculations are performed with two sills, with one placed at x = 0, and the other a distance D = 1.5km to its right. This separation is typical of sills in fjords and corresponds to that observed by Johnsson et al. (2007). The channel representing the fjord is open at its ends. In order to avoid any false reflection from the open ends of the channel, where a sponge condition is applied, the channel extends to ± 150 km. Single sill calculations with a range of grid sizes (Berntsen et al., 2008) showed that an accurate solution could be obtained with fine vertical (dz = 1m) and horizontal grid (dx of order 10m). These values were used here, although outside the sill region, dx increased gradually to 800m at the open boundary. Initial conditions corresponded to a uniform vertical temperature gradient, giving a constant buoyancy frequency $N=10^{-2}\ s^{-1}$ were applied. Motion was induced by the application of a sinusoidally varying body force, at the M_2 tidal period with Coriolis frequency $f = 1.2 \times 10^{-4}\ s^{-1}$.

Since calculations are performed on high resolution grids, minimum diffusivities (K_h, K_v) and viscosities (A_h, A_v)(with subscripts h,v denoting horizontal and vertical values) were used (XD06, Berntsen et al., 2008) to maintain numerical stability. Values were set at $K_h = K_v = 10^{-7} m^2 s^{-1}$, and $A_h = 10^{-1} m^2 s^{-1}$, $A_v = 10^{-3} m^2 s^{-1}$. However, unless molecular values and an infinitely fine high resolution grid are used then an accurate determination of the mixing is not possible. The aim here is to examine the processes that lead to small Richardson numbers and how these change between the one and two sill calculations. In addition the change in the temperature field will be quantified in terms of changes in N.

2.2 Single sill calculation.

Initially a single sill calculation was performed with the sill at x = 0. The water depth in the channel was set at h = 100m, with forcing amplitude $U_0 = 0.1 ms^{-1}$ and sill height $h_0 = 70m$, giving a sill depth $h_s = 30m$. To remove the effects of the initial conditions, the model was spun up for seven tidal cycles, and "snap shots" of the solution in the sill region at intervals of 1/8T (with T tidal period) were then examined. At t = 56/8T (the end of the seventh tidal cycle when a periodic solution was achieved) the barotropic flow to the right is a maximum and leads to an upward displacement of isotherms on the left side of the sill, and downward displacement on the right (Fig 1a). The large scale "far field" response of the sill to this barotropic tidal forcing (not presented) is to generate an internal tide which propagates away from the sill. From a "snap shot" of the "far field" distribution of currents (not shown), it is evident that away from the sill the internal tide has a wavelength of order 20km, and a 180˚ phase shift in the vertical which is typical of a first mode internal tide. In the present calculations this wavelength, λ=20km is much larger than the sill separation distance D = 1.5km. The implications of increasing D towards λ are discussed later in the paper.

In the sill region (Fig 1a), unsteady lee waves are generated (XD06), and are responsible for the small scale variability that is evident in Fig 1a. At t = 58/8T, a jet separates from the top of

the sill (Fig 1b). At this time there is significant vertical shear in the region of the top of the sill associated with the jet, that can lead to mixing (XD06). At t = 62/8T when the flow is in the opposite direction an identical jet occurs on the opposite side of the sill.

As discussed by XD06, associated with this jet and the short waves that are generated on the lee side of sills there is a region of critical Richardson number (Ri < 0.25) (Fig 1c) where there is a potential for enhanced mid-water mixing to occur. It is evident from the tidally averaged (in order to remove advection, see below) distribution of R_i and temperature field, that the temperature field at about mid-water has changed from its initial distribution. To quantify this and see how it is different in the two sill calculation, the parameter $DN = \overline{N}^2 - N_o^2$ was computed, with N_o the initial buoyancy frequency and $\overline{N}^2$ the tidally averaged buoyancy frequency value centred at t = 6.5T. It is evident from DN contours (Fig 1d) that there has been appreciable mid-water mixing at about z = -45m on either side of the sill. This mixing decreases from a maximum close to the sill. As discussed previously the model does not have a sufficiently fine grid to accurately reproduce this mixing. However, as the main aim of the paper is to see to what extent the one sill and two sill solutions differ then a comparison of the R_i and DN distribution from one and two sill calculations (see later) is useful.

A harmonic analysis of the u-component of the baroclinic velocity on the right hand side of the sill was performed (only the output at every fifth model grid was used) (Fig 2). The M_2 tidal current amplitude shows (Fig 2) a surface maximum, with amplitude decreasing away from the sill. A near-zero amplitude is evident at about mid-water, with an increase at depth. A 180˚phase change occurs in the vertical (not presented) showing the presence of a first mode baroclinic tide. Regions of surface intensification are evident at the M_4 frequency (Fig 2), with a local intensification at about mid-depth, suggesting that there are higher vertical modes in the near sill region, as shown by the rapid change in phase through the vertical (not presented). In the case of higher tidal harmonics their horizontal and vertical amplitude and phase change very rapidly, due

to the presence of short waves. Some weak beam-like structures are present in these modes. From internal tide theory, the slopes of the tidal beams are 0.8%, 2.6%, 4.2%, 5.5%, 7.0%, and 8.4% for the M_2 to M_{12} harmonics. Vertical velocity power spectra (depth integrated through the vertical) were computed. These power spectra showed significant variability in the energy in the various tidal harmonics, which changed with location, reflecting the spatial variation in the u current amplitude shown in Fig 2. For comparison with the two sill solution the power spectra at x = 750m (the location mid-way between the sills, in the two sill calculation) is given in Fig 3.

2.3 Double sill calculation

To examine to what extent the presence of a second sill at x = 1500m modifies the solution, the previous calculation was repeated with this additional sill. It is evident from Fig 1a that at t = 56/8T a region of intensified u tidal current in the upper 20m of the water column has developed between the two sills. Although at t = 58/8T there is still an intense jet that separates from the top of the right hand side of the second sill, such a jet does not occur on the right hand side of the sill at x = 0. Similarly half a tidal cycle later, namely t = 62/8T (not presented) where a jet occurs on the left hand side of the sill at x = 0, no such jet occurs on the left hand side of the sill at x = 1500m. This suggests that the second sill influences the nature of the internal waves and jet in the region between x = 0 and 1500m. In addition the isotherm separation in the region has increased. However, in terms of the large scale distribution of the internal tide, over the whole model region (not presented) this is not appreciably influenced by the presence of the second sill. In essence the second sill only influences the internal tide distribution between the sills. This is because the sill separation D = 1.5km is much shorter than the horizontal wavelength of the M_2 internal tide, namely about 20km in the present case.

Comparison of tidally averaged values of the R_i number and isotherm distributions between the one and two sill cases (Fig 1c) shows that the region of critical R_i number between the sills has significantly increased. In addition the mid-water separation of the isotherms is larger

than in the single sill calculation. Comparison of DN distributions (Fig 1d) shows that there has been substantially more mid-water mixing in the region between the two sills than found in the single sill case. This enhanced mixing has occurred despite the fact that the jet, that was present in the single sill case and was thought to be a source of mixing (XD06), is no longer present in the region between the sills. In addition this mixing is to first order horizontally uniform in the region, whereas previously it was concentrated close to the sill (Fig 1d). Although as stated previously, the model cannot accurately reproduce mixing, the presence of an enhanced region of critical R_i number in the two sill compared to the one sill calculation is indicative of a change in the mechanisms responsible for mixing.

To understand how the presence of the second sill has modified the tidal and R_i number distribution between the sills, the u component of current was harmonically analysed. In the two sill case the u current M_2 amplitude has a maximum midway between the sills, rather than close to the sill, as in the single sill case (Fig 2). As previously the M_2 current amplitude has a maximum in the surface layer, reducing to near zero close to the bed. This suggests, together with the presence of an 180˚ phase change in the vertical (not presented), that the first mode dominates.

The spatial distribution of the M_2, M_6 and M_{10} harmonics, show (Fig 2) a u current maximum amplitude, midway between the sills, although its vertical position changes from one tidal constituent to another due to different internal wave slopes, see earlier one sill discussion. In the case of two sills, the propagating internal tides from each sill can be reflected from the opposite sill and combine to form a standing internal tide. In addition for the two sill case, higher harmonics exhibit rapid vertical phase changes (not presented) showing that higher vertical modes are present, and these also contribute to changes in the vertical position of the u current maxima.

Although the M_2, M_6 and M_{10} harmonics have a maximum u current amplitude midway between the sills, for M_4 and M_8 the u current amplitude is zero mid-way between the sills. This suggests constructive and destructive interference of the internal tidal waves that propagate from each of the sills, to give standing waves between the sills. This is similar to the way in which

seiche motion of a pycnocline is formed in a lake in response to wind forcing (Hall and Davies 2005). As shown by Eriksen (1985) associated with internal wave reflection, as occurs here to form a standing wave, there is a significant increase in vertical shear and associated mixing. In the present case short wave higher harmonics of the internal tide are generated and "captured" between the sills. Consequently internal wave energy cannot propagate out of the inter-sill region and contributes to enhanced shear and reduced R_i number in this area (Fig 1c). Associated with regions in which the R_i number falls below its critical value there is enhanced mixing as quantified in the DN distributions (Fig 1d). In essence the stratification in the region between the sills reduces below the corresponding level found in the single sill case.

Associated with the standing waves between the sills there are vertical modes of increasing vertical structure (not shown). These give rise to a nodal point in the vertical velocity (w) at the centre of the region between the sills where u is a maximum at the frequency $M_{2n,}$ with n odd. This can be clearly seen in the w power spectra from the centre of the region, namely x = 750m (Fig 3b) which shows no peak at the $M_{2,}$ $M_{6,}$ M_{10} etc frequency. As previously in the single sill case at x = 750m (Fig 3a) there is a drop off in energy at frequencies higher than those associated with the internal tide. However for spectra close to the sill (not presented), in the two-sill case there is an increase in energy at the high frequency end of the spectrum. Also there is less energy in the overall internal wave spectrum for the two-sill than the single sill problem. This suggests that internal wave energy that is trapped between the sills cascades by non-linear processes into shorter internal waves and eventually mixing. It is this energy cascade that is responsible for the enhanced mixing found in the two sill calculation and observed in measurements made between closely separated sills (Johnsson et al., 2007). Since the calculations are forced at only the M_2 frequency, then the increase in energy at the high frequency end of the spectrum (Fig 3) results from an internal wave energy cascade to higher frequencies.

3. Discussion and Summary

A cross sectional non-hydrostatic model of an idealized fjord has been used to examine how the internal wave field is changed by the presence of a second sill. Calculations showed that in the region between the sills, although not outside them, the second sill influenced the intensity of the jet that detached from the lee side of the sill. In addition the nature of the internal tidal wave was changed from a progressive wave to a standing wave between the sills. Higher harmonics were generated in the form of standing waves between the sills, and there was an increase in the energy cascading to shorter wavelengths giving rise to an increase in the region of critical Richardson number and associated mixing. These changes in the region between the sills may explain the increased mixing between sills found in observations (Johnsson et al., 2007). Since the focus here has been to explain the enhanced mixing between the sills in the Ringdals fjord – Idefjord system, the sill separation D was fixed at 1.5km. However there is nothing special about this value. Additional calculations (not presented) showed that standing internal tides and enhanced mixing persisted as D was increased upto the point where D was comparable with the wavelength of the internal tide generated at a single sill (in this case 20km). Naturally as D was increased beyond this, interaction between the sills reduced, and the solution converged to the single sill case. A detailed discussion of this is beyond the scope of this paper, but calculations aimed at determining the role of D, upon mixing and internal tidal energy flux are in progress.

The application of a two dimensional cross section "slice" model of the form used here is appropriate in a narrow channel type of region such as a fjord where the flow is constrained by the lateral boundaries to be normal to the sill. However in terms of oceanic environments a full three dimensional model such as that of Xing and Davies (1998) would be required. Not withstanding this, these calculations suggest that when internal tides are formed in regions of the ocean where there are adjacent topographic features, such as a shelf edge and offshore seamount, which were shown by Xing and Davies (1998) to modify the internal tide, there is the possibility of enhanced regions of critical R_i number with associated implications for increased mixing. However, in order

to test this a full three dimensional non-hydrostatic high resolution model would be required. Increased mixing in such regions will have important implications for oceanic circulation and climate. In large scale climate models these effects can not be resolved, and they will need to be parameterized. In addition to validate such mixing parameterizations in these important regions of complex topography, it will be essential to make the key measurements in these areas.

References

Berntsen, J., Xing, J. and Davies, A.M. (2008) Numerical studies of flow over a sill: sensitivity of the non-hydrostatic effects to the grid size (submitted).

Eriksen, C. C. (1985) Implication of ocean bottom reflection for internal wave spectra and mixing. Journal of Physical Oceanography 15, 1145-1156.

Hall, P. and Davies, A.M. (2005) Effect of coastal boundary resolution and mixing upon internal wave generation and propagation in coastal regions. Ocean Dynamics, 55, 248-271.

Johnsson, M., Green, J.A.M., and Stigebrandt, A. (2007) Baroclinic wave drag from two closely spaced sills in a narrow fjord as inferred from basin water mixing. Journal of Geophysical Research, 112, C11002, doi:10.1029/2006JC003694.

New, A. L. and J. C. B. Da Silva (2002) Remote-sensing evidence of the local generation of internal solition packets in the central Bay of Biscay. Deep-Sea Research I, 49,915-934.

Van Haren, H., L. Maas, and H. Van Aken (2002) On the nature of internal wave spectra near a continental slope, Geophysical Research Letters, 29(12), 1615, doi : 10.1029/2001GLO14341.

Vlasenko, V., Stashchuk, N. and Hutter, K. (2005) Baroclinic tides. Theoretical modelling and observational evidence. Cambridge University Press.

Xing, J and Davies, A.M. (1998) A three-dimensional model of internal tides on the Malin-Hebrides shelf and shelf edge. Journal of Geophysical Research, 103, 27,821-27,847.

Xing, J. and Davies, A.M. (2005), Influence of a cold water bottom dome on internal wave trapping, Geophysical Research Letters, 32, L03601, doi : 10.1029/2004GL021833.

Xing, J., and Davies, A.M. (2006) Influence of stratification and topography upon internal wave spectra in the region of sills, Geophysical Research Letters, 33, L23606, doi : 10.1029/2006GL028092.

Zhai, X., R. J. Greatbatch, and J. Zhao (2005), Enhanced vertical propagation of storm induced near-inertial energy in an eddying ocean channel model, Geophysical Research Letters, 32, L18602, doi : 10.1029/2005GL023643.

Figure Captions

Figure 1: Sub-domain of the sill region, showing temperature field (˚C, and contour interval, c.i. = 0.5˚) and u velocity (cm s^{-1}) at (a) t = 56/8T, and (b) t = 58/8T (with T the tidal period) also for (c) the tidally averaged temperature field (˚C, and contour interval, c.i. = 0.5˚) and tidally average Richardson number (R_i) and (d) tidally averaged change in the buoyancy frequency $DN = \left(\overline{N}^2 - {N_0}^2\right) \times 10^{-4} s^{-2}$ for (left) flow over a single sill, and (right) flow over two sills.

Figure 2: Sub-domain of the sill region, showing amplitude (cms^{-1}) of the u component of the baroclinic velocity for (i) M_2, (ii) M_4, (iii) M_6, (iv) M_8, and (v) M_{10} components of the tide for (a) flow over a single sill and (b) flow over two sills.

Figure 3: Depth integrated power spectra of vertical velocity w at frequencies normalized with respect to the M_2 tide at x = 750m for (a) flow over a single sill, and (b) flow over two sills.

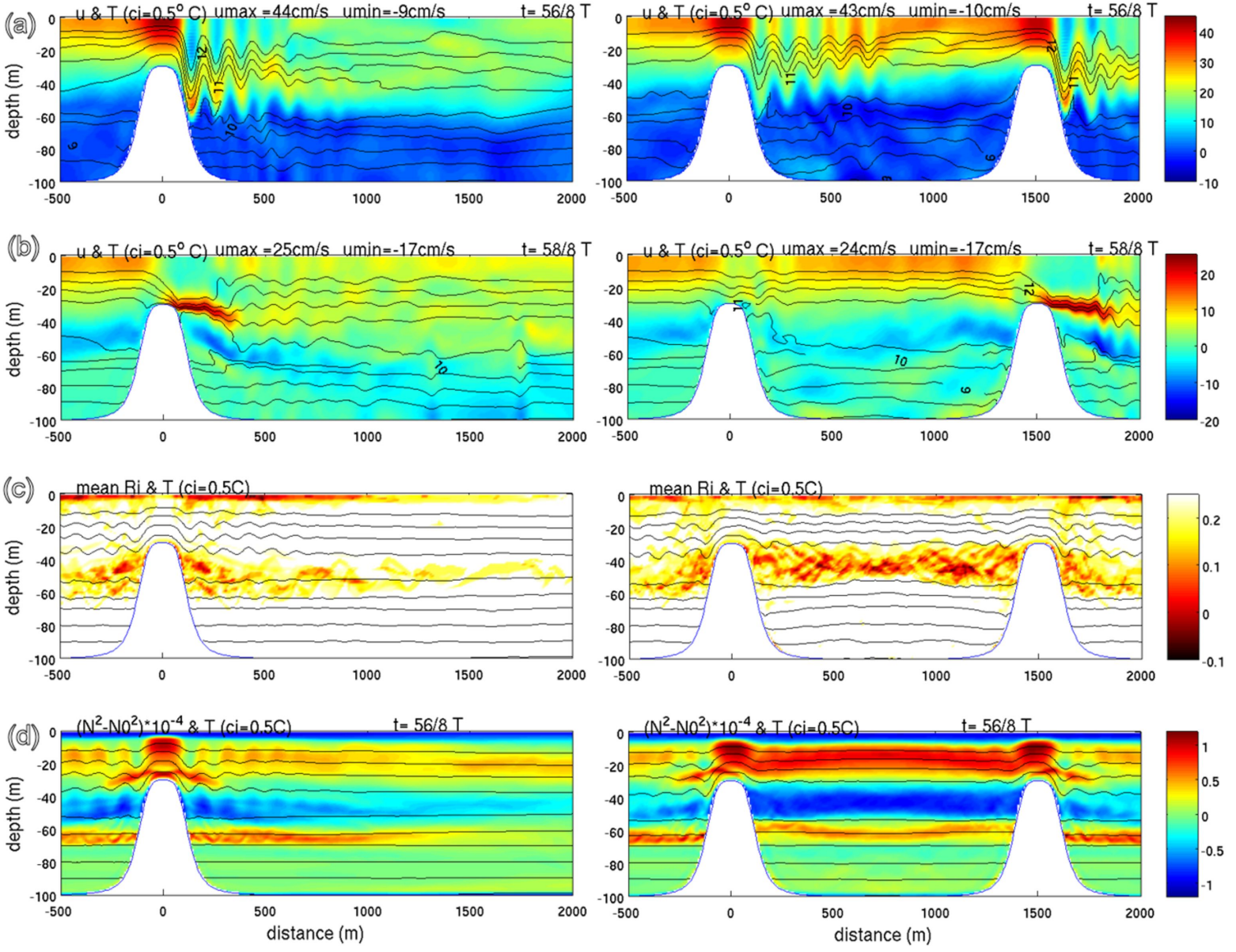
(a)
u & T (ci=0.5° C) umax =44cm/s umin=-9cm/s
t= 56/8 T
u & T (ci=0.5° C) umax =43cm/s umin=-10cm/s
t= 56/8 T
(b)
u & T (ci=0.5° C) umax =25cm/s umin=-17cm/s
t= 58/8 T
u & T (ci=0.5° C) umax =24cm/s umin=-17cm/s
t= 58/8 T
(c)
mean Ri & T (ci=0.5C)
mean Ri & T (ci=0.5C)
(d)
(N2-N02)*10-4 & T (ci=0.5C)
t= 56/8 T
(N2-N02)*10-4 & T (ci=0.5C)
t= 56/8 T
depth (m)
distance (m)
distance (m)

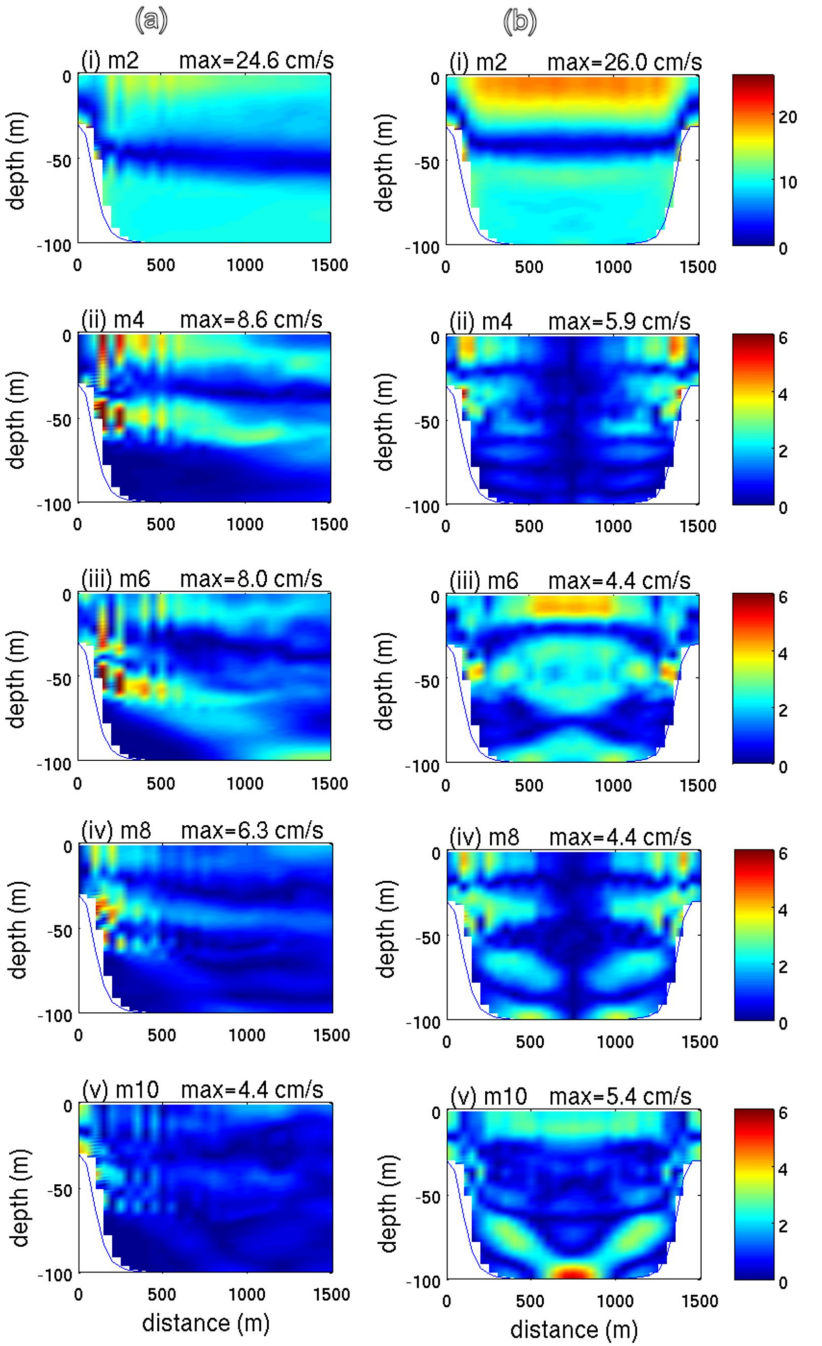
(a)
(b)
(i) m2 max=24.6 cm/s
(i) m2 max=26.0 cm/s
(ii) m4 max=8.6 cm/s
(ii) m4 max=5.9 cm/s
(iii) m6 max=8.0 cm/s
(iii) m6 max=4.4 cm/s
(iv) m8 max=6.3 cm/s
(iv) m8 max=4.4 cm/s
(v) m10 max=4.4 cm/s
(v) m10 max=5.4 cm/s
depth (m)
distance (m)
0
-50
-100
500
1000
1500
20
10
6
4
2

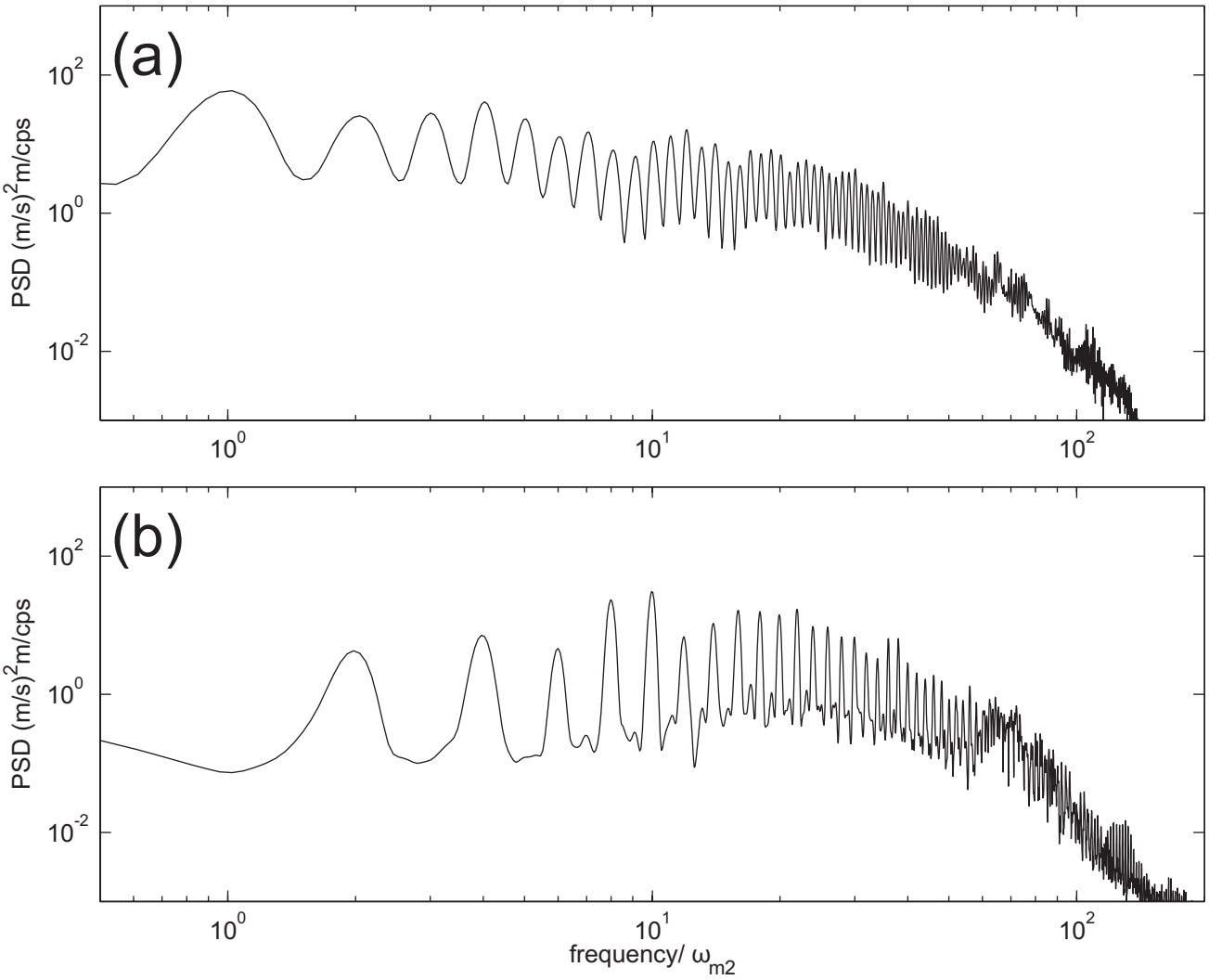
(a)
(b)
PSD (m/s)^{2}m/cps
10^2
10^0
10^{-2}
10^0
10^1
10^2
frequency/ ω_{m2}